

CHAPTER 1
Introduction
CHAPTER 2
Machining Dynamics
CHAPTER 3
Robust Control Approach
CHAPTER 4
Hardware-in-the-Loop Test System for Machining Emulation



ลิขสิทธิ์มหาวิทยาลัยเชียงใหม่
Copyright© by Chiang Mai University
All rights reserved

CHAPTER 5

Structural Dynamics: Modelling and Identification

A mathematical model of the test system was developed in order to predict the vibration behaviour prior to construction. In particular, it was necessary to be able to predict the natural frequencies of the test system structure for the dominant modes. By using finite element methods, a complete model for structural vibration was obtained. As well as using this model for verification of the system design, the model can be converted to state space form for use later in the controller design. This chapter describes the modelling process. To improve the modelling of the system, system identification methods were considered, and these are also described.

5.1 Finite Element Method

For modelling purposes, the structure, as shown in Figure 5.1 [88], can be subdivided into several beam elements which are identified by number i ($i = 1, 2, 3, \dots, n$). The element i has length l_i , cross section area A_i , mass per volume (density) ρ_i , Young's modulus E_i and cross-section area moment of inertia. Note that the structure is made from two types of material: steel (for spindle and cutting tool) and aluminium (for both flexure pivots).

The structure elements are treated as simple beam elements for vibration modelling (Figure 5.2). We adopt the Euler-Bernoulli model of beam bending. By using Galerkin method [89], the finite element formulation with the consistent mass and stiffness matrices are obtained. Considering each beam element, there I_i are two nodes for element i indexed by i and $i+1$. Hence, for n elements the final node will be numbered $n+1$. Let v_i and θ_i be the linear displacement and angular displacement at the nodal point of the element.

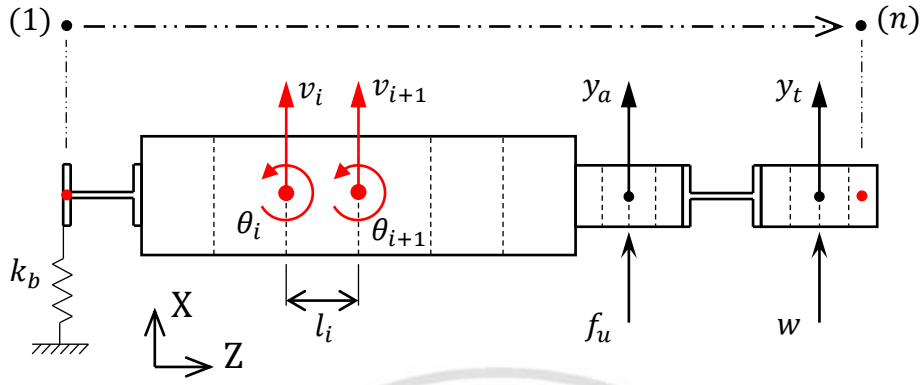


Figure 5.1 Test rig finite element model

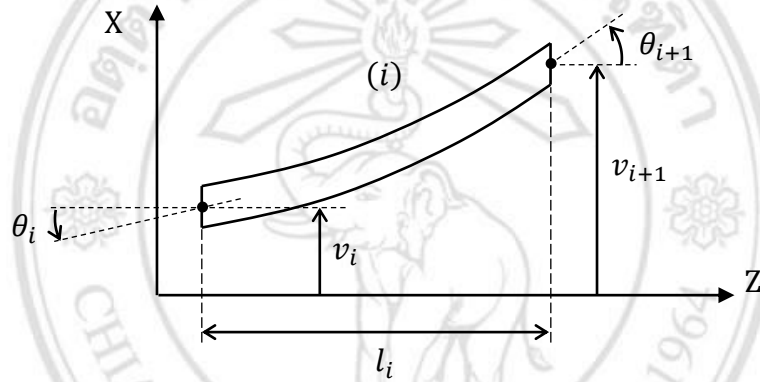


Figure 5.2 Deflection of beam element in X-Z plane

The element equation of motion may be expressed [89]:

$$M^{(i)} \ddot{\xi}^{(i)} + K^{(i)} \xi^{(i)} = f_R^{(i)} + f_{ext}^{(i)} \quad (5.1)$$

where superscript (i) indicates the element number and $M^{(i)}$ is the consistent mass matrix and $K^{(i)}$ is the stiffness matrix as given by

$$M^{(i)} = \frac{\rho_i A l_i}{420} \begin{bmatrix} 156 & 22l_i & 54 & -13l_i \\ & 4l_i^2 & 13l_i & -3l_i^2 \\ & & 156 & -22l_i \\ sym & & & 4l_i^2 \end{bmatrix} \text{ and } K^{(i)} = \frac{E_i I_i}{l_i^3} \begin{bmatrix} 12 & 6l_i & -12 & 6l_i \\ & 4l_i^2 & -6l_i & 2l_i^2 \\ & & 12 & -6l_i \\ sym & & & 4l_i^2 \end{bmatrix}.$$

The element nodal displacement vector is

$$\xi^{(i)} = [v_i \quad \theta_i \quad v_{i+1} \quad \theta_{i+1}]^T.$$

The reactive/internal nodal force vector is

$$f_R^{(i)} = \begin{bmatrix} -S_i^R & -M_i^R & S_{i+1}^R & M_{i+1}^R \end{bmatrix}^T$$

where S^R is the nodal internal shearing force and M^R is the nodal internal bending moment. An additional external nodal force vector may act on the element and can be written

$$f_{ext}^{(i)} = \begin{bmatrix} -S_i^{ext} & -M_i^{ext} & S_{i+1}^{ext} & M_{i+1}^{ext} \end{bmatrix}^T$$

where S^{ext} is the nodal external shearing force and M^{ext} is the nodal external bending moment.

To obtain the overall system mass and stiffness matrices and the internal/external force vectors the following steps are undertaken:

□ **FE model example:** Two element system

Consider the combination of two element which are element $i=1$ and element $i=2$. The external forces and bending moments act on the nodes as shown in [Figure 5.3](#). The mass and stiffness matrices for each element are given by (5.1) and have the general form

$$M^{(i)} = \begin{bmatrix} m_{11}^{(i)} & m_{12}^{(i)} & m_{13}^{(i)} & m_{14}^{(i)} \\ & m_{22}^{(i)} & m_{23}^{(i)} & m_{24}^{(i)} \\ & & m_{33}^{(i)} & m_{34}^{(i)} \\ sym & & & m_{44}^{(i)} \end{bmatrix} \text{ and } K^{(i)} = \begin{bmatrix} k_{11}^{(i)} & k_{12}^{(i)} & k_{13}^{(i)} & k_{14}^{(i)} \\ & k_{22}^{(i)} & k_{23}^{(i)} & k_{24}^{(i)} \\ & & k_{33}^{(i)} & k_{34}^{(i)} \\ sym & & & k_{44}^{(i)} \end{bmatrix}.$$

The combined system equation of motion for element 1 and element 2 can be written in the form

$$M^{(sys)} \ddot{\xi}^{(sys)} + K^{(sys)} \xi^{(sys)} = f_R^{(sys)} + f_{ext}^{(sys)}. \quad (5.2)$$

Where, for the assembled system, the mass and stiffness matrices are

$$M^{(sys)} = \begin{bmatrix} m_{11}^{(1)} & m_{12}^{(1)} & m_{13}^{(1)} & m_{14}^{(1)} & 0 & 0 \\ & m_{22}^{(1)} & m_{23}^{(1)} & m_{24}^{(1)} & 0 & 0 \\ & & m_{33}^{(1)} + m_{11}^{(2)} & m_{44}^{(1)} + m_{12}^{(2)} & m_{13}^{(2)} & m_{14}^{(2)} \\ & & & m_{44}^{(1)} + m_{22}^{(2)} & m_{23}^{(2)} & m_{24}^{(2)} \\ sym & & & & m_{33}^{(2)} & m_{34}^{(2)} \\ & & & & & m_{44}^{(2)} \end{bmatrix}$$

and

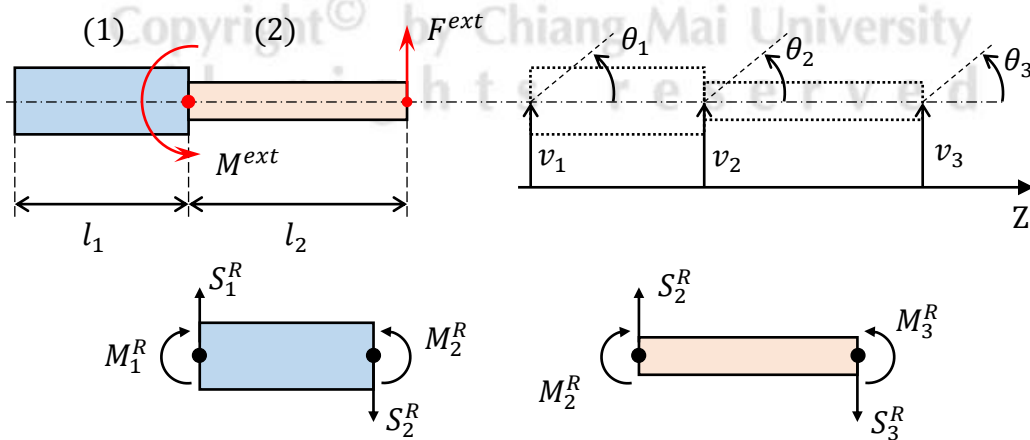


Figure 5.3 FE model elements for two-element system with external forces

$$K^{(sys)} = \begin{bmatrix} k_{11}^{(1)} & k_{12}^{(1)} & k_{13}^{(1)} & k_{14}^{(1)} & 0 & 0 \\ & k_{22}^{(1)} & k_{23}^{(1)} & m_{24}^{(1)} & 0 & 0 \\ & & k_{33}^{(1)} + k_{11}^{(2)} & k_{44}^{(1)} + k_{12}^{(2)} & k_{13}^{(2)} & k_{14}^{(2)} \\ & & & k_{44}^{(1)} + k_{22}^{(2)} & k_{23}^{(2)} & k_{24}^{(2)} \\ & & & & k_{33}^{(2)} & k_{34}^{(2)} \\ sym & & & & & k_{44}^{(2)} \end{bmatrix}.$$

The system nodal displacement vector is

$$\xi^{(sys)} = [v_1 \quad \theta_1 \quad v_2 \quad \theta_2 \quad v_3 \quad \theta_3]^T.$$

The summed (internal) system force vector is

$$f_R^{(sys)} = \begin{bmatrix} -S_1^R \\ -M_1^R \\ S_2^R - S_2^R \\ M_2^R - M_2^R \\ -S_3^R \\ -M_3^R \end{bmatrix} = \begin{bmatrix} -S_1^R \\ -M_1^R \\ 0 \\ 0 \\ S_3^R \\ M_3^R \end{bmatrix}.$$

The external system force vector acting on the system can be written

$$f_{ext}^{(sys)} = [-S_1^{ext} \quad -M_1^{ext} \quad S_2^{ext} \quad M_2^{ext} \quad S_3^{ext} \quad M_3^{ext}]^T.$$

For the example case in Figure 5.3, there are two external forces: the external moment M^{ext} acting on node 2 and the external force F^{ext} acting on node 3. Thus, the external system force vector may written

$$f_{ext}^{(sys)} = [0 \quad 0 \quad 0 \quad M^{ext} \quad F^{ext} \quad 0]^T = E_M M^{ext} + E_F F^{ext}$$

where $E_{M/F}$ are chosen to allocate the forces at the appropriated nodes. For the present example $E_M = [0 \quad 0 \quad 0 \quad 1 \quad 0 \quad 0]^T$ and $E_F = [0 \quad 0 \quad 0 \quad 0 \quad 1 \quad 0]^T$. \square

According to the FE modelling example, a complete model for the test system structure comprises $2(n+1)$ equations of motion for n elements. With the previously defined external (actuation) forces (see Figure 5.1), the resulting model has the matrix form

$$M\ddot{\xi} + K\xi = E_R f_R + E_u f_u + E_w w. \quad (5.3)$$

The nodal coordinate vector for the system has the form

$$\xi = [v_1 \quad \theta_1 \quad \dots \quad v_{n+1} \quad \theta_{n+1}]^T$$

where the vector dimension will be $(2n+2) \times 1$. Thus, the mass and stiffness matrices of the system are square with dimensions $(2n+2) \times (2n+2)$. If the structure is assumed to be fixed at the end of the base flexure, linear and angular displacements at the first node are zero ($v_1 = 0$, $\theta_1 = 0$). Then, the number of coordinates and equations of motion can be reduced by 2.

The final model includes an additional damping matrix C to account for material damping, as follows

$$M\ddot{\xi} + C\dot{\xi} + K\xi = E_u f_u + E_w w. \quad (5.4)$$

Typically, for structural vibration modelling it is convenient to assume that proportional damping arises in the form $C = \alpha M + \beta K$ where, α and β are constant values [90].

5.2 Local PD Feedback Control

Consider the external force due to actuator 1, which appears in the term $E_u f_u$ in (5.4). The force f_u can be treated as a summation of three components due to (1) negative stiffness (f_{neg}), (2) PD feedback of local position measurements (u_{PD}) and (3) additional control force which is from the optimized control design (u). Hence, we may write

$$f_u = f_{neg} + u_{PD} + u.$$

The negative stiffness force f_{neg} depends on the linear displacement at the actuator 1, which can be written in terms of the nodal displacement vector so that $E_u f_{neg} = -K_s \xi$ where

$$K_s = k_s E_u C_{a\xi} = k_s \begin{bmatrix} 0 & & & & \\ & \ddots & & & \\ & & 1 & & \\ & & & \ddots & \\ & & & & 0 \end{bmatrix}$$

where the 1 appears on the 45th diagonal matrix entry. The displacement at the actuator is $y_a = C_{a\xi}\xi$ and the negative stiffness value k_s may be calculated as shown in Section 4.3.1. Therefore, the system equation of motion with control inputs can be written in the form

$$M\ddot{\xi} + C\dot{\xi} + (K + K_s)\xi = E_u u_{PD} + E_u u + E_w w. \quad (5.5)$$

As described in Chapter 4, an initial stabilizing controller is implemented which uses PD feedback of measured displacements close to the actuators. This control scheme is shown in Figure 4.12. Note that the negative stiffness effects from actuator 2 are not included in the model as it is assumed that PD feedback is implemented to exactly cancel these effects. Hence, the net force from the actuator under PD control is zero and w is the additional force applied to emulate the cutting force excitation.

The system model in (5.5), can be changed to the state-space form by defining state variables as $v = \begin{bmatrix} \xi^T & \dot{\xi}^T \end{bmatrix}^T$. Then

$$\begin{aligned} \dot{v} &= A_v v + B_{vu} u_{PD} + B_{vu} u + B_{vw} w \\ y_a &= C_{va} v \end{aligned} \quad (5.6)$$

where $A_v = \begin{bmatrix} 0 & I \\ -M^{-1}(K + K_s) & -M^{-1}C \end{bmatrix}$, $B_{vu} = \begin{bmatrix} 0 \\ -M^{-1}E_u \end{bmatrix}$, $B_{vw} = \begin{bmatrix} 0 \\ -M^{-1}E_w \end{bmatrix}$.

The PD control force for the magnetic actuator may be expressed $u_{PD} = -(K_P y_a + K_D \dot{y}_a)$. For implementation, a filtered derivative is employed so that, in the Laplace domain, the PD controller is

$$U_{PD}(s) = \left(-K_P - \frac{K_D s}{\tau_D s + 1} \right) Y_a(s). \quad (5.7)$$

This can be realized in the state space form

$$\begin{aligned}\dot{x}_{PD} &= A_{PD}x_{PD} + B_{PD}y_a \\ u_{PD} &= C_{PD}x_{PD} + D_{PD}y_a.\end{aligned}\quad (5.8)$$

Combining (5.6) and (5.8), the system model with PD control is

$$\dot{\nu} = A_{\nu}\nu + B_{\nu u}u + B_{\nu w}w \quad (5.9)$$

where $A_{\nu} = \begin{bmatrix} A_v + B_{\nu u}D_{PD}C_{\nu a} & B_{\nu u}C_{PD} \\ B_{PD}C_{\nu a} & A_{PD} \end{bmatrix}$, $B_{\nu u} = \begin{bmatrix} B_{\nu u} \\ 0 \end{bmatrix}$, $B_{\nu w} = \begin{bmatrix} B_{\nu w} \\ 0 \end{bmatrix}$, and the state vector

is $\nu = [\nu^T \quad x_{PD}^T]^T$. The system outputs are the displacements at the actuators, expressed in terms of state variables as $y_a = C_{\nu a}\nu$ and $y_t = C_{\nu t}\nu$ where y_a is the displacements at the control actuator (actuator 1) and y_t is the displacement at the tool tip (actuator 2).

The steps for the FEM modelling process for the flexible structure under PD control can be summarized as follows:

- a) Segment the ‘spindle’ structure into elements according to the cross-section and the type of material, for which the element equations of motion are given by (5.1).
- b) Combine elements by considering interaction forces to obtain the flexible structure model in the form (5.3).
- c) Eliminate the zero vibration nodes at the clamped end and include a linear damping property to give the form in (5.4).
- d) Consider the components of the force from actuator 1 to account for the negative stiffness effect, leading to the state space model as shown in (5.6).
- e) Combine the PD controller with filter derivative in state space form (5.8) leading to the model of flexible structure under PD control as (5.9).

5.3 FE Method with PD Control: Numerical Results

According to the flexible structure details shown in Figure 5.4 with the parameter values given in Table 5.1, and with the actuator and sensor properties already described in Section 4.2, a complete system model was obtained in the form of (5.9). From the eigenvalues of the matrix A_{ν} in (5.9) the natural frequencies for the first three modes

are $\omega_{n1} \approx 204$ rad/sec, $\omega_{n2} \approx 546$ rad/sec and $\omega_{n3} \approx 1503$ rad/sec. From the corresponding eigenvectors of A_v , the mode shapes for the flexible structure vibration are determined and are shown in Figure 5.5. From the three mode shapes, we can describe that the 1st mode is the main pitching mode with bending mainly at the base flexure and only small deflection of the tool end. This will be referred to as the ‘rigid body mode’. The 2nd mode involves significant deflection of the tool end, and for this reason will be referred to as the ‘tool bending mode’. The other higher frequency modes involve more complex distortion of the flexures with significant shearing.

The frequency response of the system under PD control may be calculated based on the state space description (5.9). The output measurement must be defined according to the sensor positions, as previously described. Thus, the transfer function for the complete structure model has the form similar to (4.8) with $f_1 = u$ and $f_2 = w$. So we have

$$\begin{bmatrix} Y_a(s) \\ Y_t(s) \end{bmatrix} = G_{FE}(s) \begin{bmatrix} U(s) \\ W(s) \end{bmatrix}. \quad (5.10)$$

Where the transfer function matrix (based on FE modelling) is

$$G_{FE} = \begin{bmatrix} C_{va} \\ C_{vt} \end{bmatrix} [sI - A_v]^{-1} \begin{bmatrix} B_{vu} & B_{vw} \end{bmatrix} = \begin{bmatrix} g_{y_a u}^{FE} & g_{y_a w}^{FE} \\ g_{y_t u}^{FE} & g_{y_t w}^{FE} \end{bmatrix}.$$

The frequency response plot of the flexible structure covering the first six resonant modes is shown in Figure 5.6. It can be seen that the natural frequency values are quite well matched with the experimental data given in Chapter 4 (Figure 4.15). According to Figure 5.6, the cutting transfer function $g_{y,w}^{FE}$, shows two significant modes of vibration within a nominal range of frequencies for operation and vibration control of 0-1000 rad/s (which corresponds to tooth-pass frequencies 0-160 Hz).

We can investigate the effectiveness of the PD controller to improve the cutting stability boundary by considering the cutting transfer function $g_{y,w}^{FE}$ as described for $G(s)$ in Section 2.3. The derivative gain (K_D) is varied to maximize the damping ratio for the tool bending mode (see feedback structure shown in Figure 5.7). Note that it is the tool bending mode that has the main impact on the form of the stability lobe

boundary for stable cutting. The main drawback for applying PD control to a flexible structure, is that there is a pinning effect of localized control that will limit the achievable damping. This can be seen from the root locus diagram for varying K_D , as shown in Figure 5.8. High gain values drive the closed-loop poles toward the open loop zero locations. The frequency response for $g_{y,w}^{FE}$ is shown in Figure 5.9 for a range of K_D values. This result demonstrated the effect of the resonance peak for the tool bending mode for $K_D = 5 \rightarrow 20$ Ns/m which is in accordance with the root locus diagram in Figure 5.8. For the optimal damping value the stability limit was predicted to be $b_{K,\max} = 339$ N/mm. This is, however, a significant improvement over the base-level PD control for which $b_{K,\max} = 180$ N/mm.

Table 5.1 Parameters value of the flexible structure

parts mane	symbol	length (mm)	number of element	area, $b \times h$ (mm ²)	material
flexure pivot 1	l_6	5	1	25×35	aluminum
	l_7	30	6	2.5×35	
	l_8	5	1	25×35	
spindle	l_1	187.5	8	45×45	steel
	l_2	10	2	45×45	
	l_3	15	2	25×45	
	l_4	25	6	25×45	
	l_5	10	2	25×45	
flexure pivot 2	l_6	5	1	25×25	aluminum
	l_7	30	6	2.5×25	
	l_8	5	1	25×25	
tool tip	l_9	10	2	25×35	aluminum
	l_{10}	25	6	25×35	steel
	l_{11}	10	2	25×35	aluminum

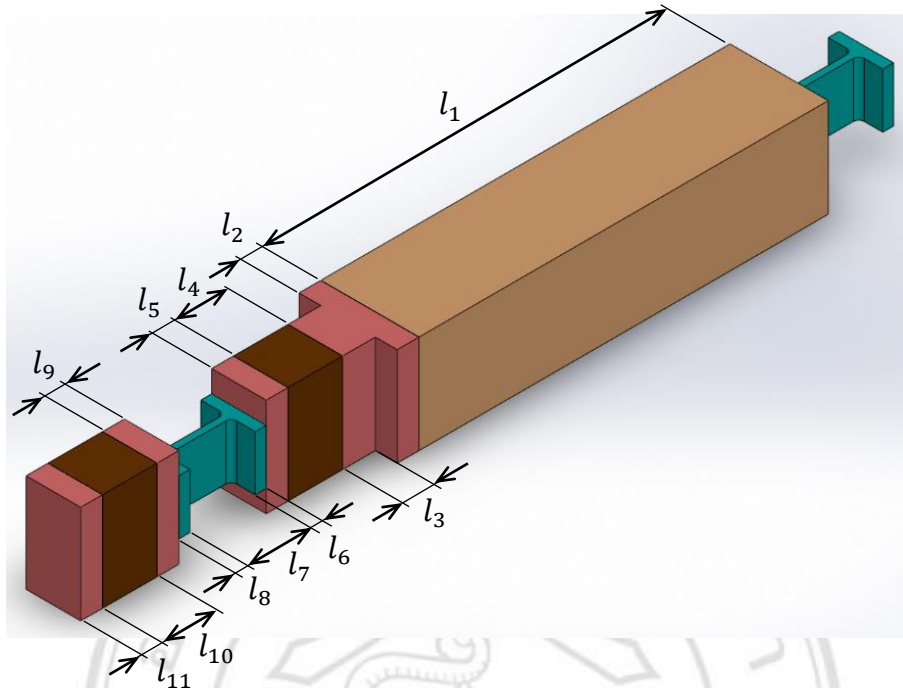


Figure 5.4 Detail of the flexible structure element

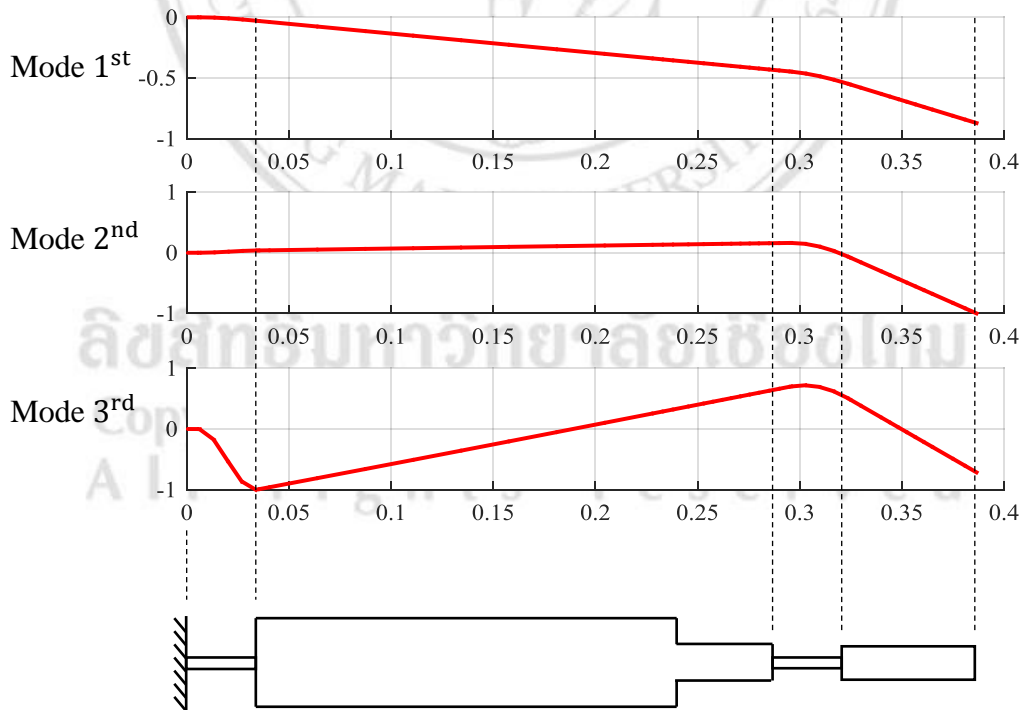


Figure 5.5 Mode shape of flexible structure for first three modes

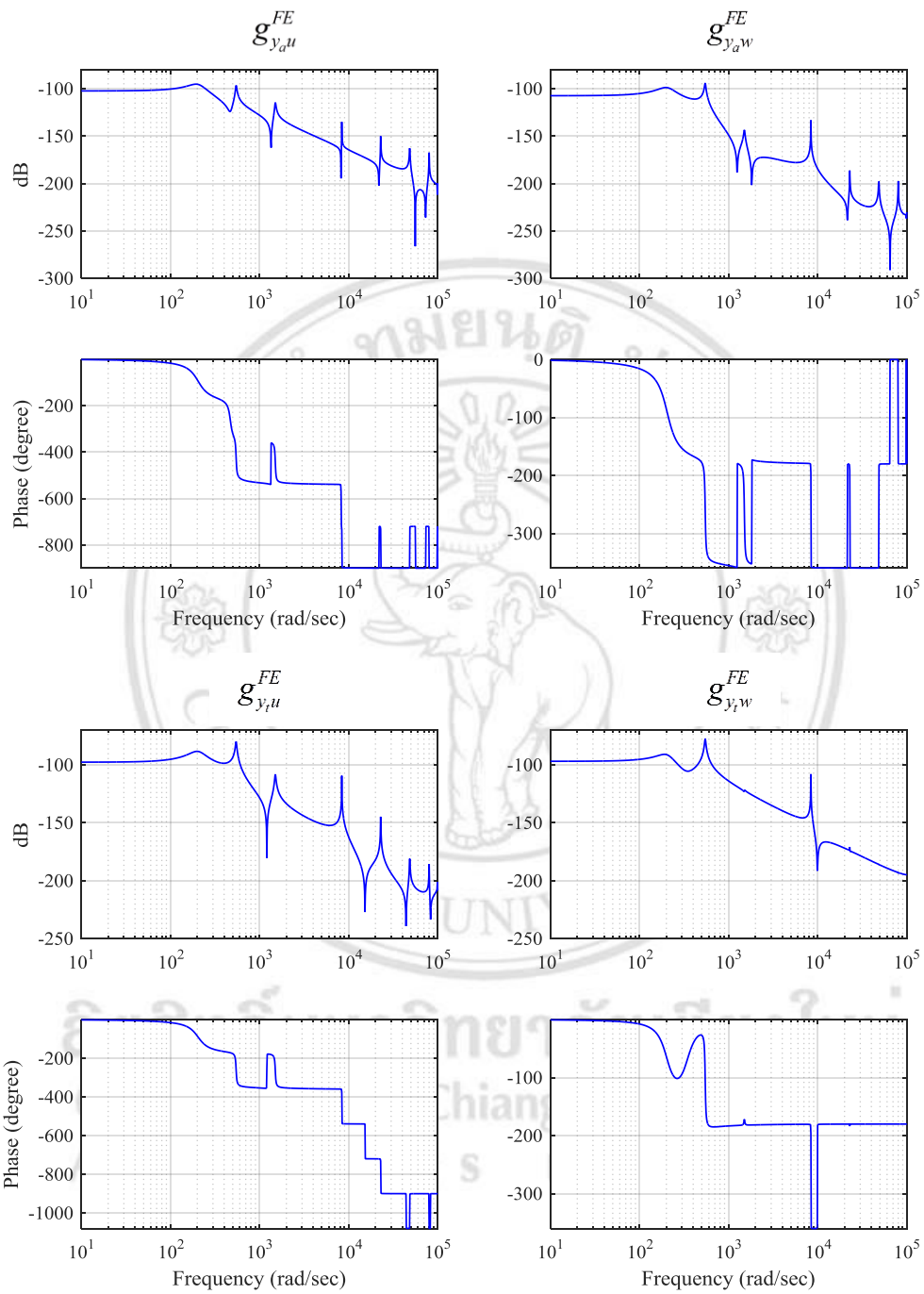


Figure 5.6 Frequency response of FE model with PD controller

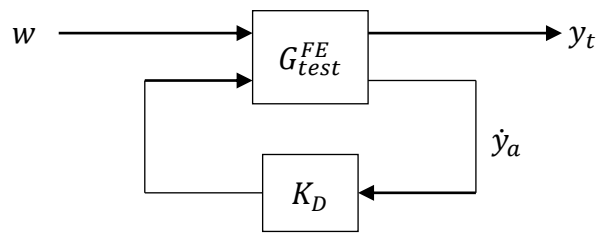


Figure 5.7 Changing derivative gain K_D plant scheme

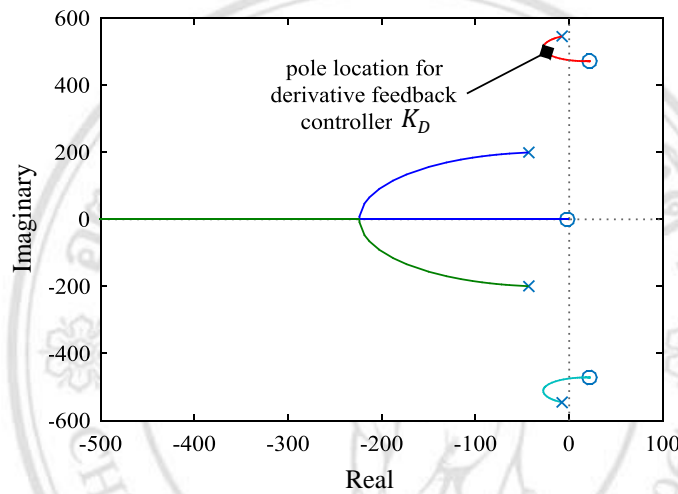


Figure 5.8 Root Locus for changing derivative gain feedback K_D

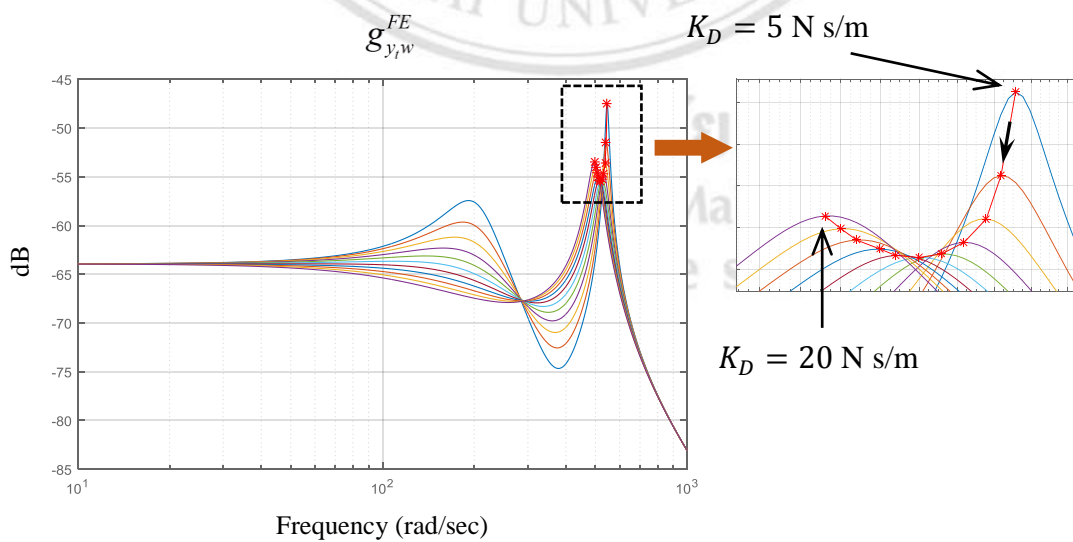


Figure 5.9 Flexible structure frequency response with PD derivative gain varied $K_D = 5 - 20$ Ns/m

5.4 Modal Analysis and Model Reduction

A main issue for numerical analysis and controller synthesis is the computational complexity for high order models. Therefore, it is advantageous if the flexible structure model with PD controller in (5.9), which is very high order (186 states), can be transformed to a reduced order representation. This model must be accurate over a frequency range covering the natural frequencies modes of the rigid body mode and tool bending mode.

5.4.1 Similarity transformations

Consider a general state space model in the form

$$\begin{aligned}\dot{x} &= Ax + Bu \\ y &= Cx.\end{aligned}$$

The transfer function is $H(s) = C(sI - A)^{-1}B$. Now, define the arbitrary invertible matrix T , and the new state vector

$$\hat{x} = Tx.$$

So that the new states in the vector \hat{x} are simply a linear combination to the old states in vector x . Due to T is a constant matrix and $x = T^{-1}\hat{x}$, we have

$$\begin{aligned}\dot{\hat{x}} &= T\dot{x} = TAx + TBu = TAT^{-1}\hat{x} + TBu \\ y &= Cx = CT^{-1}\hat{x}.\end{aligned}$$

Define the new variables, $\hat{A} = TAT^{-1}$, $\hat{B} = TB$ and $\hat{C} = CT^{-1}$ then the new state space model has the form as

$$\begin{aligned}\dot{\hat{x}} &= \hat{A}\hat{x} + \hat{B}u \\ y &= \hat{C}\hat{x}.\end{aligned}$$

The transfer function corresponding to this model is given by

$$\begin{aligned}\hat{H}(s) &= \hat{C}(sI - \hat{A})^{-1}\hat{B} = CT^{-1}(sI - TAT^{-1})^{-1}TB \\ &= CT^{-1}(sTT^{-1} - TAT^{-1})^{-1}TB \\ &= CT^{-1}T(sI - A)^{-1}T^{-1}TB \\ &= C(sI - A)^{-1}B \\ &= H(s).\end{aligned}$$

So that, the transfer function of the old model $H(s)$ is the same as the transfer function of the new model $\hat{H}(s)$. The transformation $\hat{A} = TAT^{-1}$ is called a *similarity transformation*. Since, both of the matrices set of (A, B, C) and $(\hat{A}, \hat{B}, \hat{C})$ produce the same transfer function $H(s)$ and the poles of $H(s)$ are the eigenvalues of A and \hat{A} thus the following relationship holds: “The eigenvalues of A are the same as the eigenvalues of $\hat{A} = TAT^{-1}$ for invertible matrix T ”. This is a well know result in matrix theory.

5.4.1 Modal form transformation

For analysis, it is useful to apply a similarity transformation (as in Section 5.4.1) to obtain a Jordan canonical form. There are three types of Jordan canonical form as follows [91]:

- 1) If the matrix A has distinct and real eigenvalues $\lambda_1 \lambda_2 \dots \lambda_n$ then we can find the transformation matrix T such that

$$\hat{A} = TAT^{-1} = \begin{bmatrix} \lambda_1 & & & 0 \\ & \lambda_2 & & \\ & & \ddots & \\ 0 & & & \lambda_n \end{bmatrix}$$

where T is formed from the eigenvectors of the matrix of A :

$$T = [v_1 \ v_2 \ \dots \ v_n]$$

with the column vector v_i being the eigenvector corresponding to the eigenvalue λ_i satisfying $Av_i = \lambda_i v_i$.

- 2) If the matrix A has repeated and real eigenvalues (for which it may be assumed that the repeated eigenvalue λ_1 is repeated k times), then there are two cases which must be considered according to $\text{rank}(\lambda_1 I - A) = l$:

- 2.1) If $n - l = k$ that means the eigenvector matrix has the form

$$T = [v_1 \ v_2 \ \dots \ v_n]$$

where $v_1 \dots v_k$ are independent eigenvectors corresponding to λ_1 . The Jordan canonical form is given by

$$\hat{A} = TAT^{-1} = \begin{bmatrix} \lambda_1 & & & 0 \\ & \lambda_2 & & \\ & & \ddots & \\ 0 & & & \lambda_n \end{bmatrix}$$

where $\lambda_1 = \lambda_2 = \dots = \lambda_k$.

2.2) If $n-l < k$ there are less than k independent eigenvectors corresponding to λ_1 . We can solve this case by let v^0 be an the eigenvector of λ_1 then the generalized eigenvector can be obtain by solving by

$$\begin{aligned} (A - \lambda_1 I)v^1 &= v^0 \\ (A - \lambda_1 I)v^2 &= v^1 \\ &\vdots \\ (A - \lambda_1 I)v^k &= v^{k-1}. \end{aligned}$$

Therefore, the generalized eigenvector has the form

$$T = [v^0 \quad v^1 \quad \dots \quad v^{k-1} \quad \dots \quad v_n].$$

The obtained Jordan canonical form is no longer diagonal, and has some terms of value 1 above the diagonal

$$\hat{A} = TAT^{-1} = \begin{bmatrix} \lambda_1 & 1 & & & 0 \\ & \lambda_2 & \ddots & & \\ & & \ddots & 1 & \\ & & & \ddots & \lambda_k \\ 0 & & & & \lambda_n \end{bmatrix}$$

3) If the matrix A has complex conjugate eigenvalues given by $\lambda_1, \lambda_2 = \sigma \pm j\omega$. Then the corresponding eigenvector must also appear as the complex conjugate pair $v_1, v_2 = p \pm jq$. Then, the transformation matrix has the form

$$T = [p \quad q \quad v_3 \quad \dots \quad v_n].$$

Giving the Jordan canonical form as follows

$$\hat{A} = TAT^{-1} = \begin{bmatrix} \sigma & \omega & & 0 \\ -\omega & \sigma & & \\ & & \lambda_3 & \\ & & & \ddots \\ 0 & & & & \lambda_n \end{bmatrix}.$$

Consider the test system model as presented in (5.9), with $\dot{v} = A_v v + B_{vu} u + B_{vw} w$. A set of output measurements may be defined according to sensor location (at actuator 1 and 2) in the form $y_m = C_{mv} v$ where

$$y_m = [y_a \quad y_t \quad \dot{y}_a \quad \dot{y}_t]^T.$$

The eigenvalues calculated for the matrix A_v with size $n \times n$ include both complex conjugate pairs and real values and can be written in the form

$$\lambda_i = \sigma_1 \pm j\omega_1, \sigma_2 \pm j\omega_2, \dots, \sigma_k \pm j\omega_k, \lambda_{k+1}, \dots, \lambda_n$$

and the corresponding eigenvectors also appear as the complex conjugates:

$$v_i = p_1 \pm jq_1, p_2 \pm jq_2, \dots, p_k \pm jq_k, v_{k+1}, \dots, v_n.$$

Then, the transformation matrix has the form

$$T = [p_1 \quad q_1 \quad p_2 \quad q_2 \quad \dots \quad p_k \quad q_k \quad v_{k+1} \quad \dots \quad v_n].$$

Consequently, the Jordan canonical form is

$$\hat{A}_v = TA_v T^{-1} = \begin{bmatrix} \sigma_1 & \omega_1 & & & & & & & 0 \\ -\omega_1 & \sigma_1 & & & & & & & \\ & & \sigma_2 & \omega_2 & & & & & \\ & & -\omega_2 & \sigma_2 & & & & & \\ & & & & \ddots & & & & \\ & & & & & \sigma_k & \omega_k & & \\ & & & & & -\omega_k & \sigma_k & & \\ & & & & & & & v_{k+1} & \\ & & & & & & & & \ddots \\ 0 & & & & & & & & & v_n \end{bmatrix}.$$

This gives the modal form model defined as

$$\begin{aligned}\dot{\hat{v}} &= \hat{A}_v \hat{v} + \hat{B}_{vu} u + \hat{B}_{vw} w \\ y_m &= \hat{C}_{mv} \hat{v}\end{aligned}\quad (5.11)$$

where $\hat{A}_v = TA_v T^{-1}$, $\hat{B}_{vu} = TB_{vu}$ and $\hat{C}_{mv} = C_{mv} T^{-1}$.

5.4.2 Reduced order model

From the modal form system in (5.11) there is a clear decoupling of states for each mode. Therefore, model reduction can be performed by a direct elimination of states i.e. by retaining sub-matrices of $\hat{A}_v = TA_v T^{-1}$, $\hat{B}_{vu} = TB_{vu}$ and $\hat{C}_{mv} = C_{mv} T^{-1}$.

As the operational frequencies for control on the test system are restricted to below 700 rad/sec approximately, we consider the map of pole values and enclosing circle of radius 700 rad/s, as shown in Figure 5.10. Therefore, we will retain only the two lowest frequency modes (rigid body mode and tool bending mode) in the model which is defined as

$$\begin{aligned}\dot{x}_R &= A_R x_R + B_{Ru} u + B_{Rw} w \\ y_m &= C_{mR} x_R.\end{aligned}\quad (5.12)$$

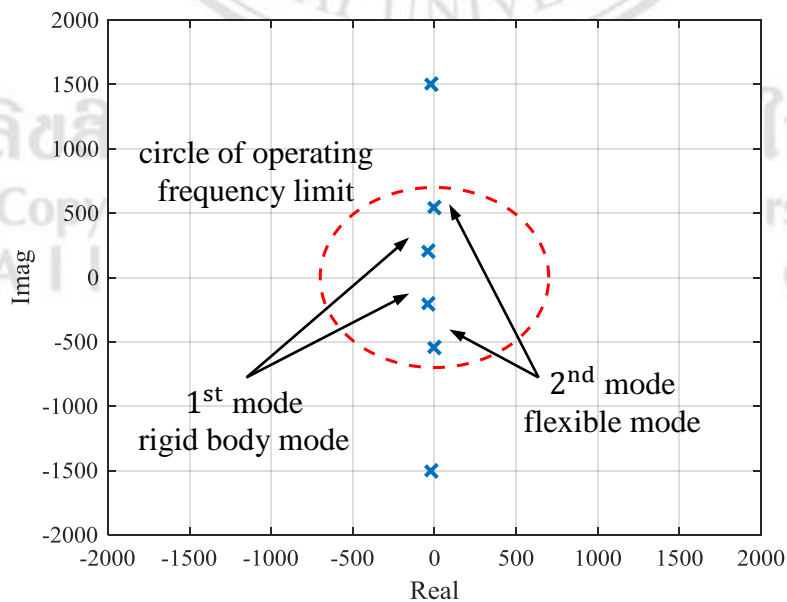


Figure 5.10 Poles location of \hat{A}_v with the operating frequency limit of the test rig

The reduced state vector x_R has size 4×1 and the model matrices having compatible dimensions. Note that the number of states matches the size of the measurement output y_m and thus the matrix C_{mR} is a square matrix.

As a further transformation, we may transform the system states so that they match the measured variables ($x = y_m$) by using the transformation $x_R = C_R^{-1}x$. In this case,

$$\begin{aligned} C_{mR}^{-1}\dot{x} &= A_R C_{mR}^{-1}x + B_{Ru}u + B_{Rw}w \\ y_m &= C_{mR} C_{mR}^{-1}x. \end{aligned}$$

And so the reduced system form with direct state measurement is

$$\begin{aligned} \dot{x} &= Ax + B_u u + B_w w \\ y &= Cx \end{aligned} \quad (5.13)$$

where $A = C_{mR} A_R C_{mR}^{-1}$, $B_u = C_{mR} B_{Ru}$, $B_w = C_{mR} B_{Rw}$ and C is the 4×4 identity matrix.

For the test system, the numerical values for the model matrices in (5.13) are

$$A = \begin{bmatrix} 0 & 0 & 1 & 0 \\ 0 & 0 & 0 & 1 \\ -135526 & 50792 & -149 & 0.33 \\ 322230 & -212343 & -25.3 & 46.35 \end{bmatrix}, \quad B_w = \begin{bmatrix} 0 \\ 0 \\ 24.1 \\ 5.26 \end{bmatrix} \quad \text{and} \quad B_u = \begin{bmatrix} 0 \\ 0 \\ 1.55 \\ 54.5 \end{bmatrix}. \quad (5.14)$$

We can now compare the full order model in (5.9) and the final model to be used for analysis and controller synthesis in (5.13) in terms of the frequency response. For the reduced model (5.13) we define the transfer function matrix as follows

$$\begin{bmatrix} Y_a(s) \\ Y_t(s) \end{bmatrix} = G(s) \begin{bmatrix} U(s) \\ W(s) \end{bmatrix} \quad (5.15)$$

The transfer function matrix is

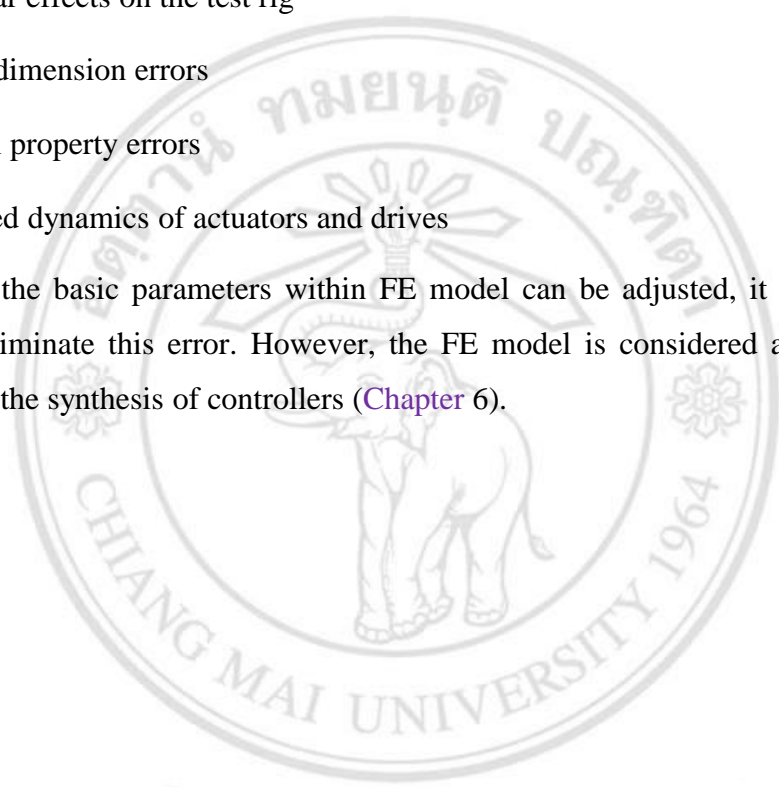
$$G = \begin{bmatrix} C_a \\ C_t \end{bmatrix} [sI - A]^{-1} [B_u \quad B_w] = \begin{bmatrix} g_{y_a u} & g_{y_a w} \\ g_{y_t u} & g_{y_t w} \end{bmatrix}.$$

A comparison of the frequency responses to confirm the final model accuracy with the full order model is shown in Figure 5.11. It is clear that a good match is

obtained over the frequency range of operation. For further validation it is necessary to compare the reduced order model with the measured test system frequency response as shown in [Figure 5.12](#). It can be seen that the resonant frequencies of the reduced order model are consistent with the measurements from the test system. Some errors can be seen in the frequency response which may be due to various factors including

- the dynamics of FE model is a linear model which cannot account for some nonlinear effects on the test rig
- test rig dimension errors
- material property errors
- neglected dynamics of actuators and drives

Even though the basic parameters within FE model can be adjusted, it is difficult to completely eliminate this error. However, the FE model is considered acceptable for further use in the synthesis of controllers ([Chapter 6](#)).



ลิขสิทธิ์มหาวิทยาลัยเชียงใหม่
Copyright© by Chiang Mai University
All rights reserved

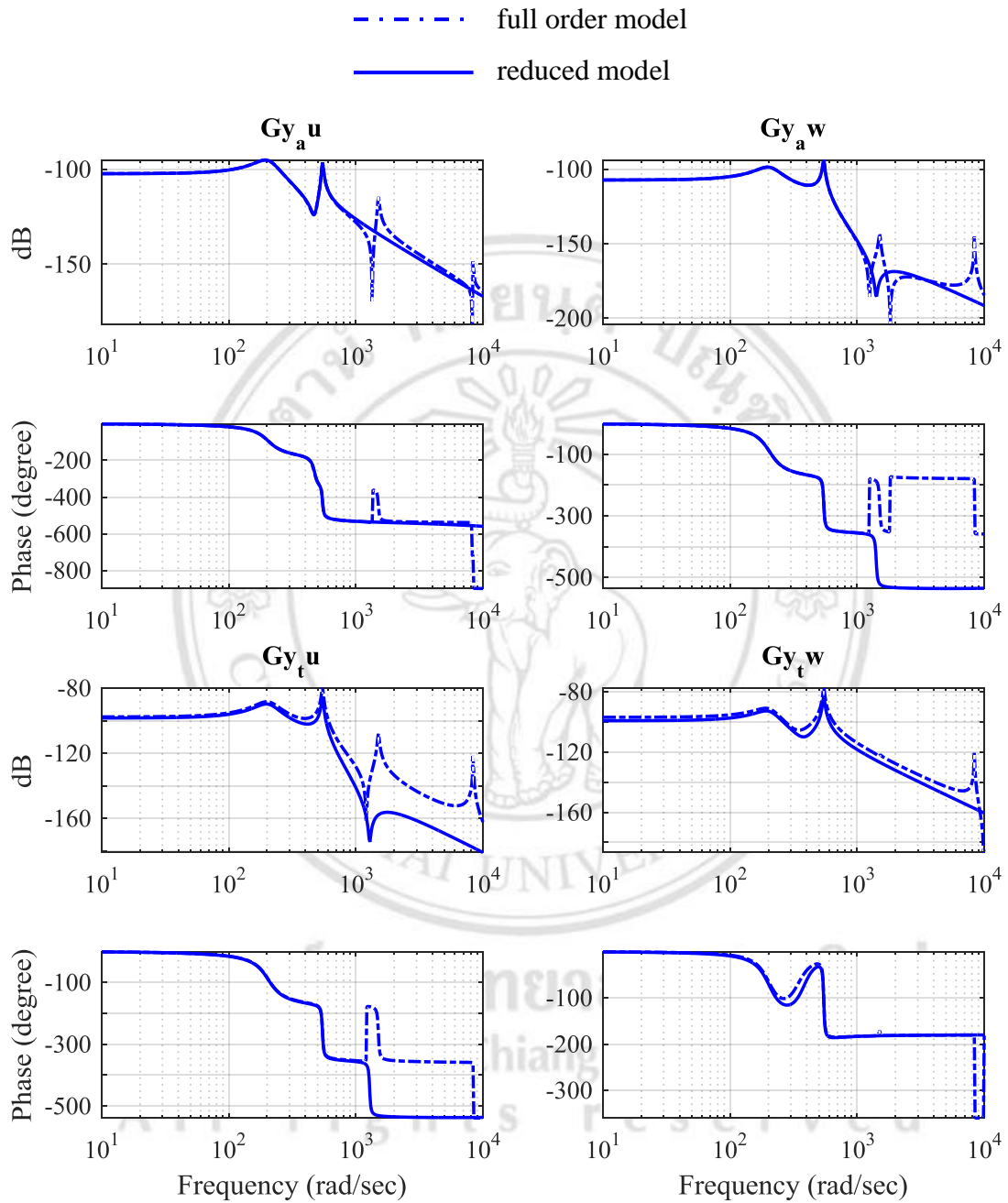


Figure 5.11 Frequency response from FE modelling comparing the full order model versus the reduced order model

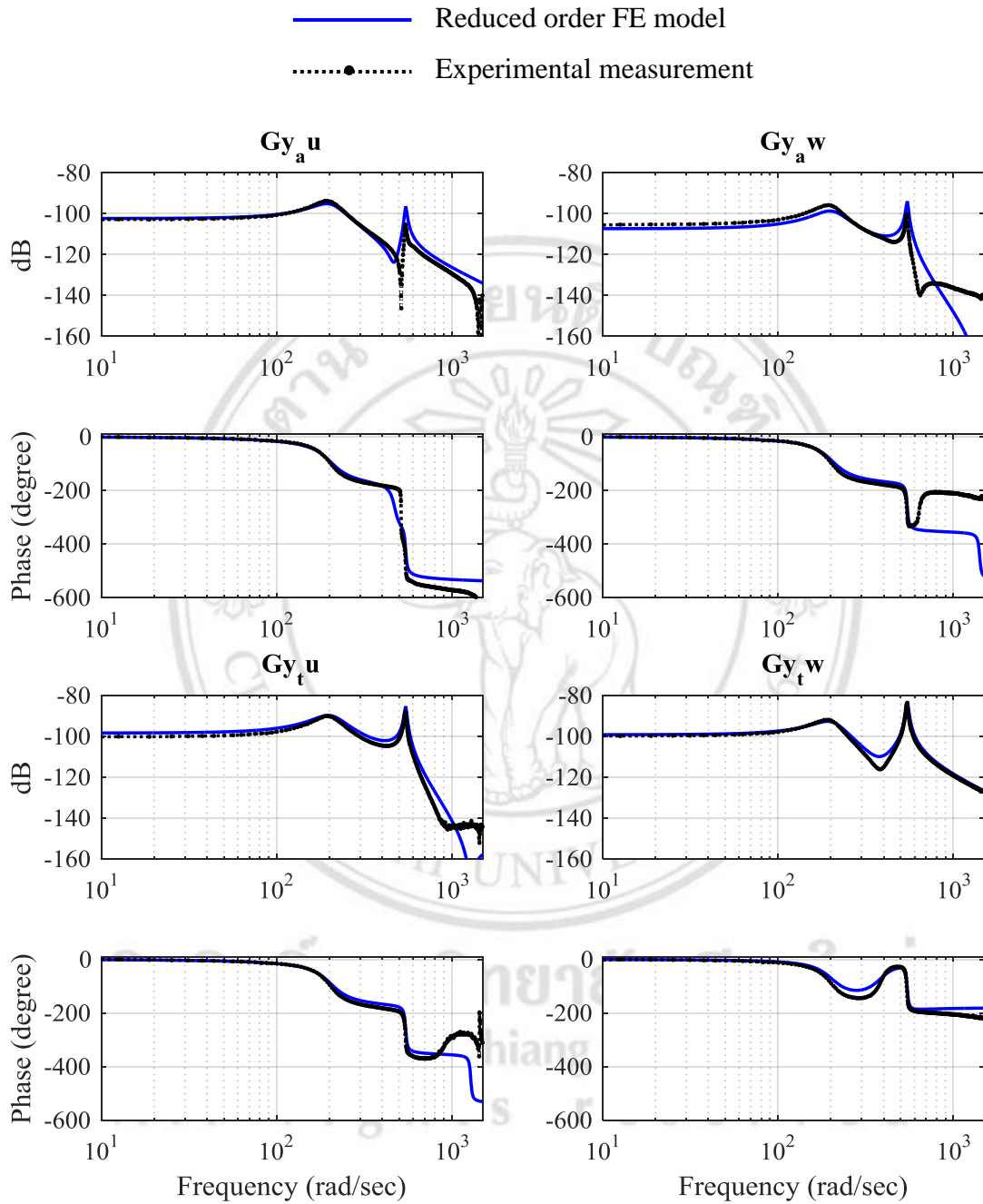


Figure 5.12 Frequency response comparing reduced order FE model and experimental results from direct testing

5.5 System Identification and Model Improvement

Preliminary modelling and design work for the test system was done using FEM as described in Section 5.1. After the test system was built, the comparative results in Figure 5.12 were obtained. In order to obtain an improved accuracy of the system model it is possible to use the test system frequency response data and apply system identification methods. Although the physical basis for the model is then lost, the potentially higher accuracy is of benefit when synthesizing the designed controllers. The methods used to identify the system model were based on the system identification toolbox in the MATLAB® software program [92].

The complete set of output measurements considered for analysis and control include the displacement and velocity of the test system structure at the actuator locations. We can write the I/O relation of the test system in matrix transfer function form as

$$\begin{bmatrix} Y_a(s) & Y_t(s) \end{bmatrix}^T = G_{test}^{ID}(s) \begin{bmatrix} U(s) \\ W(s) \end{bmatrix} \quad (5.16)$$

where the transfer function here relates to an identification model and has the form

$$G_{test}^{ID} = \begin{bmatrix} g_{y_a, u} & g_{y_a, w} \\ g_{y_t, u} & g_{y_t, w} \end{bmatrix} \quad (5.17)$$

The frequency response data corresponding to G_{test}^{ID} as already presented in Section 4.6 by (4.8). The identification model can be obtained directly from the frequency response data using the system ID toolbox in MATLAB® [92]. For the system ID model we define the state space representation as:

$$\begin{aligned} \dot{x}_{id} &= A_{id} x_{id} + B_{id, u} u + B_{id, w} w \\ y &= C_{id} x_{id}. \end{aligned} \quad (5.18)$$

Now, we can also use the similarity transformation in order to transform the reduced model to the state-output model by the state transformation $x_{id} = C_{id}^{-1} x$, which yields

$$\begin{aligned}\dot{x} &= Ax + B_u u + B_w w \\ y &= Cx.\end{aligned}\tag{5.19}$$

where $A = C_{id} A_{id} C_{id}^{-1}$, $B_u = C_{id} B_{id,u}$, $B_w = C_{id} B_{id,w}$ and $C = I$. The matrix values in (5.19) are

$$A = \begin{bmatrix} -70.4 & 10 & 1.02 & 0.02 \\ -19.5 & -18.7 & -0.041 & 1.08 \\ -79943.3 & 29002.2 & -15.9 & -4.72 \\ 293904.4 & -239228.2 & -13.6 & 24.43 \end{bmatrix}, B_u = \begin{bmatrix} 0 \\ 0 \\ 19.2 \\ 7.2 \end{bmatrix} \text{ and } B_w = \begin{bmatrix} 0 \\ 0 \\ 8.93 \\ 45.38 \end{bmatrix}\tag{5.20}$$

The comparison of the frequency responses for the 4th order and 8th order identified models and (5.19) are shown in Figure 5.13. These results show that the 8th order model from system ID has very low error compared with the measured frequency response data. The reduced system ID model shows larger errors, particularly for higher frequencies but would have advantages for controller synthesis and implementation, in terms of numerical complexity. Furthermore, it can be seen that the system ID models have higher accuracy than the FE model. Therefore, the system ID models are the most suitable for synthesizing the designed controllers.

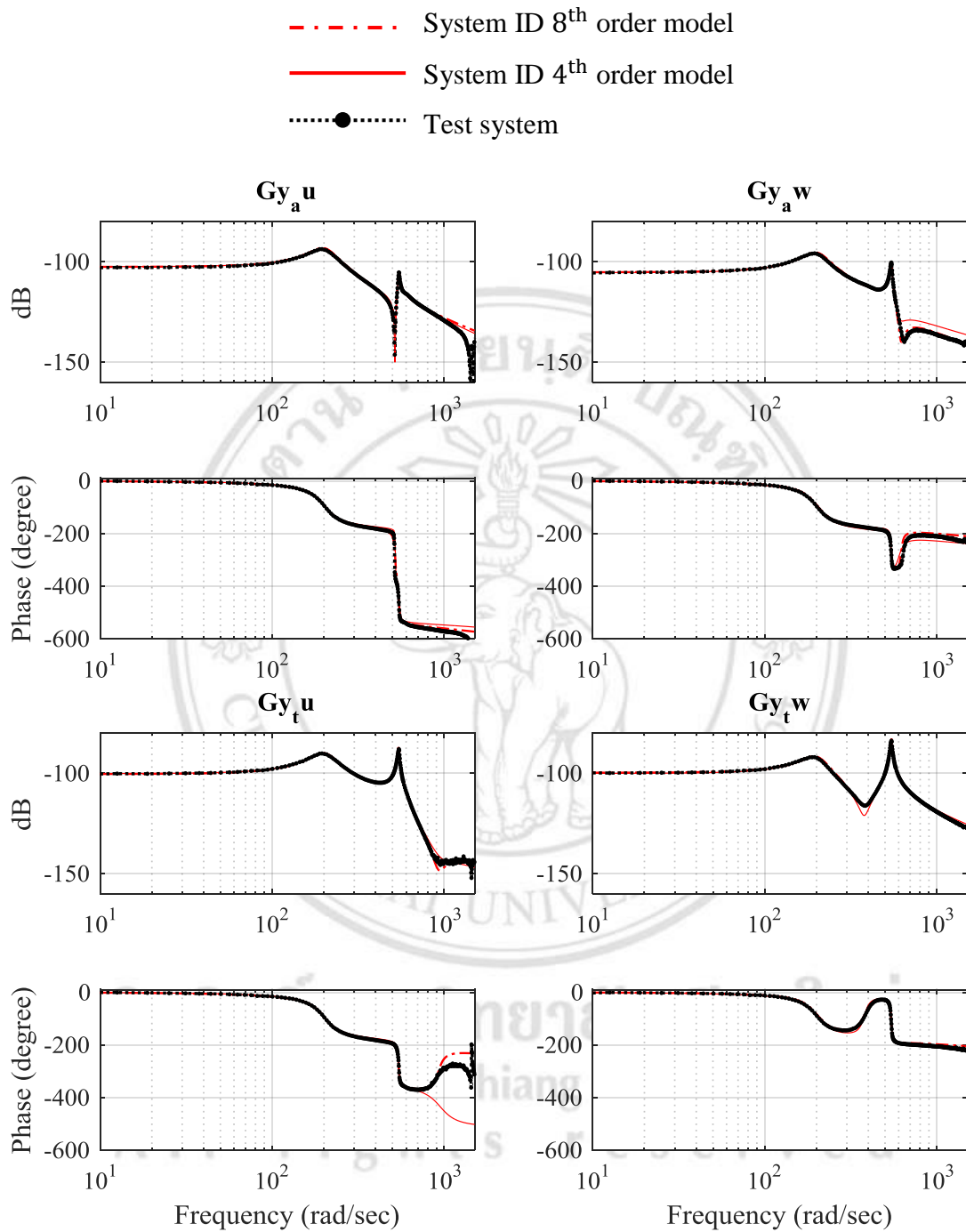


Figure 5.13 Frequency response results for three cases, (i) 8th order system ID model, (ii) reduced 4th order system ID model, (iii) test system measured data



ลิขสิทธิ์มหาวิทยาลัยเชียงใหม่
Copyright© by Chiang Mai University
All rights reserved